A study of a new class of discrete nonlinear Schrödinger equations

2002 J. Phys. A: Math. Gen. 35 8109

(http://iopscience.iop.org/0305-4470/35/38/312)

INSTITUTE OF PHYSICS PUBLISHING JOURNAL OF PHYSICS A: MATHEMATICAL AND GENERAL

J. Phys. A: Math. Gen. **35** (2002) 8109–8133 PII: S0305-4470(02)37499-7

A study of a new class of discrete nonlinear Schrödinger equations

K Kundu

Institute of Physics, Bhubaneswar 751 005, India

Received 29 May 2002
Published 12 September 2002
Online at stacks.iop.org/JPhysA/35/8109

Abstract

A new class of 1D discrete nonlinear Schrödinger Hamiltonians with tunable nonlinearities is introduced, which includes the integrable Ablowitz–Ladik system as a limit. A new subset of equations, which are derived from these Hamiltonians using a generalized definition of Poisson brackets, and collectively referred to as the N-AL equation, is studied. The symmetry properties of the equation are discussed. These equations are shown to possess propagating localized solutions, having the continuous translational symmetry of the one-soliton solution of the Ablowitz–Ladik nonlinear Schrödinger equation. The N-AL systems are shown to be suitable for studying the combined effect of the dynamical imbalance of nonlinearity and dispersion and the Peierls–Nabarro potential, arising from the lattice discreteness, on the propagating solitary wave-like profiles. A perturbative analysis shows that the N-AL systems can have discrete breather solutions, due to the presence of saddle centre bifurcations in phase portraits. The unstaggered localized states are shown to have positive effective mass. On the other hand, large-width but small-amplitude staggered localized states have negative effective mass. The collision dynamics of two colliding solitary wave profiles is studied numerically. Notwithstanding colliding solitary wave profiles that are seen to exhibit nontrivial nonsolitonic interactions, certain universal features are observed in the collision dynamics. The future scope of this work and possible applications of the N-AL systems are discussed.

PACS numbers: 05.45.Yv, 05.60.Cd, 52.35.Mw, 63.20.Ls, 63.20.Pw

1. Introduction

As is well known, different nonlinear models can possess spatially localized solutions for solitary waves [1–3]. In many cases, the solitary waves are analysed in the framework of integrable models which, however, describe realistic physical systems with certain approximations [4]. Two important examples of integrable nonlinear equations are the

nonlinear Schrödinger (NLS) equation and the sine-Gordon (s-G) equation. While the first one is known to form 'dynamical solitons', the last one yields 'kink' and 'antikink' solutions. These are also called 'topological solitons' [1]. Dynamical solitons arise from the acute balance of nonlinearity and dispersion. The origin of topological solitons is the balance of nonlinearity and constraints from topological invariants [1, 5]. Alongside these continuous equations, a pioneering example of an integrable discrete differential equation is the Ablowitz–Ladik equation. This is often referred to as the integrable discretization of continuous NLS (ALDNLSE) [6–8]. On the other hand, the standard discretization of NLS gives the nonintegrable discrete nonlinear Schrödinger equation (DNLSE) [9–11].

The utility of the ALDNLSE in the analysis of physical problems is rather tortuous. Consider, for example, physically motivated models, such as coupled nonlinear atomic strings with onsite or intersite anharmonic potentials [12], an array of coupled optical waveguides [13], proton dynamics in hydrogen-bonded chains [4, 14–16], the Davydov and Holstein models (DHM) for transport in biophysical systems [2, 4, 16], and so on. In these models, either the ALDNLSE does not appear at all or it does not appear in its pristine form. However, to study the soliton dynamics perturbatively in these models, the ALDNLSE is the appropriate choice for the zeroth-order approximation [12, 13, 16, 17]. This clearly shows that the ALDNLSE is an equation of great significance in nonlinear science. For other applications of this equation we mention the following examples. The dynamics of low-frequency and high-frequency intrinsic localized modes in nonlinear lattices can be described to a good approximation by the ALDNLSE [18, 19]. Again, in the study of dark and bright excitons in systems with exchange and dipole–dipole interactions, it is shown that in some limiting cases the evolution equations resulting from model Hamiltonians are reduced to the exactly integrable ALDNLSE [20]. As another example, we cite the one-dimensional Frölich model of exciton(vibron)–phonon interaction. This model can be approximated by the ALDNLSE, provided we are interested in the dynamics of large-width and small-amplitude dynamical solitons [16]. One other important use of the ALDNLSE lies in the numerical integration of the NLS. This is done to avoid any numerical instability problem [6].

Any small perturbation may break the integrability so strongly that solitary waves can be unstable and in the extreme case may altogether disappear. The nonintegrablity in an otherwise integrable nonlinear equation can also give birth to internal modes, often called 'shape modes' in solitary waves. These internal modes can drastically modify the soliton dynamics [21]. The physical origins of integrability-breaking terms can be many. For example, this type of term can arise from taking into consideration the effect of thermal fluctuations and the possible absence of order in the system [8, 22–24]. However, the most important one is the discreteness of the underlying space. One noteworthy example of an integrable nonlinear equation that becomes nonintegrable due to discretization is the Frenkel–Kontorova (FK) model, which is the spatially discretizd s-G equation [25]. Another prominent example in this category is the already-mentioned DNLSE [9–11]. So, relevant in this context is the study of an IN-DNLS, and also the modified Salerno equation (MSE) [16, 26]. The IN-DNLS is a hybrid form of the ALDNLSE and the DNLSE with a 'tunable' nonlinearity. On the other hand, in the MSE, the usual DNLSE is replaced by a modified version of the DNLSE, the ADNLSE which involves acoustic phonons, instead of optical phonons in condensed matter physics parlance [17]. These equations are studied with the prime objective of understanding the role of lattice discreteness as a mechanism for the collapse of moving self-localized states to stable, but pinned localized states [16, 26]. We further note that an IN-DNLS, which can be continually switched from the DNLSE to the ALDNLSE by varying a single parameter, is also studied to investigate the discreteness induced oscillatory instabilities of dark solitons [27].

One important field of study in nonlinear nonintegrable equations is whether or not solitary wave-like solutions can exist in these equations. So, consider the NLS with an additional Hamiltonian perturbation that models a nonlinear interaction between Langmuir waves and electrons in plasma. It constitutes an interesting example of a continuous nonlinear nonintegrable equation, which can have solitary waves as well as periodic solutions, and recurrence. It is further observed by numerical analysis of the nonlinear equation that recurrence depends sensitively on initial conditions [28]. However, physically highly relevant and consequently most well studied example is the 'ϕ^4 equation'. This continuous nonlinear equation is nonintegrable, in contrast to its 'cousin' s-G system. This ϕ^4 equation can have either solitary wave solutions or 'kink-like' solutions with permanent profile. However, these solutions do not have the simple collision properties of solitons. These solutions can bump, lock or annihilate each other. In addition, these always emit some oscillatory disturbances or radiation in the course of a collision. Furthermore, the head-on collisions of kink and antikink pairs of solutions of the ϕ^4 equation will settle either to a bound state (bion) or to a two-soliton solution. This settling down is found to depend fractally on the impact velocity. We further note that all solutions of the ϕ^4 equation have profound physical as well as theoretical significance [29–33]. In continuation, we mention that the appearance of fractal structure in the kink–breather interaction is investigated using the FK model [25]. Similarly, a fractal structure in solitary-wave collisions for the coupled NLS equations is reported. This structure is observed in the separation velocity versus collision velocity graph [34].

Contrary to common belief, there are nonintegrable discrete systems which possess exact solitary waves. Indeed, there is also an existence theorem [35]. The key hypothesis in the proof of the existence theorem is that the interaction potential, $V(\cdot)$, should at least have superquadratic growth. Since, for the Toda lattice, $V(\phi) = ab^{-1}(\exp(-b\phi) + b\phi - 1)$, the condition is trivially satisfied. It is known that the Toda equation is integrable and it has soliton solutions [29, 36]. Nontrivial examples are, of course, cubic and quartic systems, $V(\phi) = \frac{1}{2}\phi^2 + \frac{1}{3}a\phi^3$ $(a > 0)$ and $V(\phi) = \frac{1}{2}\phi^2 + \frac{1}{4}b\phi^4$ $(b > 0)$ studied by Fermi, Pasta and Ulam (FPU) [29, 35–37]. Another example is systems having a Lennard-Jones potential, relevant for the macroscopic theory of classical fluids [35]. We again note that one important property of a spatially discretized nonlinear equation is the existence of intrinsic localized modes or discrete breathers. For brevity, we mention only the discrete nonlinear Klein–Gordon equation and FPU equations. These equations are studied extensively, albeit numerically, to show the existence, stability, mobility, reactivity and also the collisional properties of breathers [38–43]. In the case of the discrete nonlinear Klein–Gordon equation, it is found that large breathers have a tendency to take energy from smaller ones. It is also seen in the numerical analysis that once they are large enough, discrete breathers cease to absorb energy from small ones. These regulation processes prevent a collapse of the energy into a single huge excitation, which could destroy the lattice [40, 43].

Here I propose an extended nonintegrable version of the ALDNLSE, which has a 'tunable' nonlinearity in the intersite hopping term. At the same time, the form of nonlinearity is such that it can allow solitary wave-like solutions, as seen say, in the ϕ^4 equation, and its suitable parallel in the linear regime is one-dimensional correlated disordered systems [44, 45]. It is to be noted that my case is not covered by the existence theorem that I have already mentioned. Inasmuch as this nonlinearity is in the intersite hopping term, it serves two important purposes. First of all, this extra dispersive correction to the ALDNLSE will try to destroy the Ablowitz–Ladik (AL) soliton by dispersion. So, by varying this term we can investigate the effect of dispersive imbalance on the maintenance of the moving solitonic profile. It is relevant at this point to note that both the IN-DNLS and the MSE investigate the competition between the on-site trapping and the solitonic motion of the AL solitons. In the case of the MSE, it

is found that the narrow AL solitons, having width smaller than the critical width, will get pinned by the lattice potential [16, 17]. Similar results are obtained numerically from the IN-DNLS [26]. Secondly, since the extra dispersive term in the proposed equation breaks the integrability of the ALDNLSE, the dynamics of the AL solitons will not be transparent to the lattice discreteness. So, along with the IN-DNLS and the MSE, this model also gives an opportunity to study further the effect of the Peierls–Nabarro (PN) potential on the dynamics of solitons [26, 46]. We further note that the DHM yields a very complicated nonlinear discrete differential equation [16]. So, to gain a better understanding of the DHM, a somewhat simpler but physically relevant system needs to be considered [16]. This is another important motivation of this study. It is in fact noteworthy in this context that a slightly modified ALDNLSE has been studied as a plausible model for dynamical self-trapping in discrete lattices [47]. As for further motivation of this study, we note that one rapidly emerging field in nonlinear dynamics is the study of the solitary-wave interaction in nonintegrable nonlinear models. The emergence of this field is due to the possibility of observing many of the predicted effects experimentally, including soliton energy and momentum exchange [25, 29–34, 48, 49]. The model that is to be proposed here allows us to study the head-on collision of scalar lattice solitary waves. Finally, nonlinear phenomena are quite a common occurrence in all branches of natural science. But, our theoretical understanding of nonlinear equations, particularly that of nonlinear discrete differential equations is quite limited. So, when viewed from this angle, another important dimension gets added to the present study.

This paper is organized as follows. In what follows, I first propose a set of discrete nonintegrable Hamiltonians, and derive the equation of interest from the requisite Hamiltonian. I then study analytically the existence of a moving solitary wave-like solution in this equation. Since this equation is a perturbated Ablowitz–Ladik equation, I study this problem further using a standard perturbative method to find trapped and moving solitons. I consider next the formation of stationary localized states and the effective masses of these states. Subsequently, I present some numerical results to substantiate the analysis. I also study the collision of two solitary wave profiles numerically using the equation. Findings from my study are summarized at the end. In this final section, I also discuss the applicability and future scope of the present work.

2. A general derivation of the Ablowitz–Ladik class of nonlinear equations

We consider here the following Hamiltonian, H:

$$H = J\sum_n \left(\phi_n^\star\phi_{n+1} + \phi_{n+1}^\star\phi_n\right) - \frac{1}{2}\sum_n\sum_{j=1}^{l} g_0^j\left(\phi_n^\star\phi_{n+j} + \phi_{n+j}^\star\phi_n\right)^2 + \frac{2\nu}{\lambda}\sum_n |\phi_n|^2 - \frac{2}{\lambda}\left(\frac{\nu}{\lambda} - J\right)\sum_n \ln\left[1+\lambda|\phi_n|^2\right]. \tag{2.1}$$

It is understood that the Hamiltonian, H, in equation (2.1) describes a conservative system in which a quasiparticle (exciton, vibron, etc) moves in an one-dimensional chain. To obtain the time evolution equations for generalized coordinates, $\{\phi_m, \phi_m^\star\}$, we make use of the nonstandard Poisson bracket relationship among these generalized coordinates as given in appendix A. After defining $\phi_m = (-1)^m\psi_m$, we get for $m = 1, 2, \ldots$

$$\begin{aligned}\mathcal{F}_j\left(\psi_m, g_0^j\right) &= g_0^j\sum_{\sigma=\pm1}\left(\psi_m^\star\psi_{m+\sigma j} + \psi_{m+\sigma j}^\star\psi_m\right)\psi_{m+\sigma j}\\ \mathcal{F}(\psi_m,\lambda) &= \left(1+\lambda|\psi_m|^2\right)\sum_{j=1}^{l}\mathcal{F}_j\left(\psi_m, g_0^j\right)\end{aligned} \tag{2.2}$$

$$\mathrm{i}\dot{\psi}_m - 2J\psi_m + J\big(1+\lambda|\psi_m|^2\big)(\psi_{m+1}+\psi_{m-1}) = 2\nu|\psi_m|^2\psi_m - \mathcal{F}(\psi_m,\lambda). \tag{2.3}$$

In $\mathcal{F}(\psi_m,\lambda)$, arguments, g_j^0, $j=1,2,\ldots,l$ have been suppressed, and $J>0$. When $l=1$, in equation (2.1) and consequently in equation (2.3), we have just an extra nonlinear nearest-neighbour coupling in hopping with a coupling constant, g_0^1. This coupling is assumed to arise due to quasiparticle–phonon interaction [16]. Similarly, when $l=2$, we have both nonlinear nearest-neighbour and next-nearest-neighbour couplings. Coupling constants are g_0^1 and g_0^2, respectively. So, in this model coupling constants are assumed to depend on the distance between the sites involved. For any arbitrary l then, a given site, over and above the standard linear nearest-neighbour coupling, is coupled through nonlinear hopping to l consecutive sites in general on both sides of it. Of course, the origin of such coupling is assumed to arise due to the heuristic generalization of quasiparticle–phonon interaction beyond the nearest neighbour. We further note that in this model also

$$\mathcal{N} = \sum_{m=-\infty}^{\infty} \ln\big[1+\lambda|\psi_m|^2\big] = \text{constant} \tag{2.4}$$

as in the original Ablowitz–Ladik equation (see also appendix A). So, if $\lambda|\psi_m|^2 \ll 1$ for all m, we get $\sum_m |\psi_m|^2 \approx$ constant. We now consider the following limits of equation (2.3): (1) When $g_0^j = 0$ for all j, we have the Salerno equation in the quantum version. In the classical domain, it has been nomenclatured as IN-DNLS and the formation of staggered localized states from this equation is studied [26, 50, 51]. (2) When $\nu = 0$ as well as $g_0^j = 0$ for all j, we have the standard Ablowitz–Ladik equation. This equation is known to have a single-soliton solution [6, 7]. (3) When $\lambda = 0 = \nu$ and also $l = 1$, we have the model where exciton–phonon interaction affects only the hopping between nearest neighbours. Of course, to obtain this particular nonlinear mathematical form of interaction, it is assumed that the lattice relaxation is faster than the quasiparticle dynamics [16]. This is a very standard assumption which is used in the Davydov soliton [17, 52] and also in the Rashba and Toyozawa mechanism for the formation of a self-trapped exciton [53–55]. This equation is also studied for the single-soliton solution, using the perturbation method [16]. (4) The equation with $\nu = 0$ will be referred to here as the nonintegrable Ablowitz–Ladik (N-AL) equation. Consider again the situation where we take $l = 1$ in the N-AL equation and further ignore altogether in equation (2.3) the term having $g_0^1\lambda$. We have then a model equation which describes a truncated version of the model, in which exciton(vibron)–phonon interaction affects both site-energy and hopping. We note that a perturbative analysis of the full model is done for the one-soliton solution [16]. Here our plan is to analyse various aspects of the N-AL equation.

Before we proceed further, we define $\tau = Jt$, $\Psi_m = \sqrt{\lambda}\psi_m, m \in Z$, and $g_j = \frac{g_0^j}{\lambda J}$. We further note that $\mathcal{F}_j\big(\frac{\Psi_m}{\sqrt{\lambda}}, g_0^j\big) = \frac{1}{\sqrt{\lambda}}\mathcal{F}_j(\Psi_m, g_j)$, $j = 1,2,\ldots,l$. This, in turn, yields $\mathcal{F}\big(\frac{\Psi_m}{\sqrt{\lambda}},\lambda\big) = \frac{1}{\sqrt{\lambda}}\mathcal{F}(\Psi_m,1), m \in Z$. So, in the limit of $\nu = 0$, we have from equation (2.3) and $m \in Z$

$$\mathrm{i}\dot{\Psi}_m - 2\Psi_m + \big(1+|\Psi_m|^2\big)(\Psi_{m+1}+\Psi_{m-1}) = -\mathcal{F}(\Psi_m,1) \tag{2.5}$$

and equation (2.4) also remains valid with $\lambda = 1$ and ψ_m replaced by Ψ_m. Again, $\mathcal{F}(\Psi_m,1)$ should have in its argument $g_1, g_2, \ldots, g_l$, which have been suppressed for convenience. We note that equation (2.5) possesses a reflection symmetry. To understand this, we consider the transformation, $\Psi_m \to (-1)^m\Psi_m\exp(-4\mathrm{i}\tau)$. The equation will remain invariant under this transformation provided $\tau \to -\tau$ and $g_j \to -g_j$, $j \in l$. Again, if $\mathcal{F}(\Psi_m,1) = 0, m \in Z$, the equation becomes self-dual under this reflection transformation.

3. Propagating solutions of equation (2.5)

In order to gain an understanding of the nature of the solution of equation (2.5), we consider the case where $g_j = 0$ for all j. As mentioned earlier, in this limit we have the integrable Ablowitz–Ladik discrete nonlinear Schrödinger equation (ALDNLSE) [6, 7]. The exact one-soliton solution of the ALDNLSE, Ψ_m^0, $m \in Z$ is

$$\Psi_m^0(\tau) = \frac{\sinh\mu}{\cosh[\mu(m-x)]}\exp[\mathrm{i}k(m-x) - \mathrm{i}\alpha] = Q_m(\tau)\exp[\mathrm{i}k(m-x) - \mathrm{i}\alpha] \tag{3.1}$$

with the following equations for the soliton parameters:

$$\dot{\mu} = 0 \qquad \dot{k} = 0 \qquad \dot{\alpha} = \omega \tag{3.2}$$

$$\omega = 2[1 - \cosh\mu\cos k] \tag{3.3}$$

$$\dot{x} = \frac{2}{\mu}\sinh\mu\sin k. \tag{3.4}$$

So, for each μ there exists a band of velocities (see equation (3.4)) at which the localized state or the one-soliton state can travel without experiencing any PN pinning due to the lattice discreteness [26, 42, 46]. We also note that for a given k, $\mu \in [0, \infty]$. Mathematically, the one-soliton solution of the ALDNLSE describes two parameters, namely k and μ, a family of curves. So, even if we pin the value of one of those parameters to a prescribed value, equation (3.1) will still be a solution of the ALDNLSE.

We now consider $\mathcal{F}\big(\Psi_m^0, 1\big)$. Introducing equation (3.1) in equation (2.5) we get

$$\frac{\mathcal{F}\big(\Psi_m^0, 1\big)}{2\big(1+Q_m^2\big)\Psi_m^0(\tau)} = \sum_{j=1}^{l}\Big\{g_j\cos kj\Big[\big(Q_{m+j}^2 + Q_{m-j}^2\big)\cos kj + \mathrm{i}\big(Q_{m+j}^2 - Q_{m-j}^2\big)\sin kj\Big]\Big\}. \tag{3.5}$$

For convenience in further discussion, we consider only one term, say the lth term of the sum in equation (3.5). We note that for $\cos kl = 0$, permissible values of k are $k = \pi - \big(\frac{2j_1+1}{l}\big)\big(\frac{\pi}{2}\big)$, $j_1 = 0, 1, 2, \ldots, (2l-1)$. So, there are $2l$ permissible values of k for $k \in [-\pi, \pi]$. We now state the following results.

(1) For $l = 1$, $\mathcal{F}\big(\Psi_m^0, 1\big) = 0$ for $m \in Z$, if $|k| = \frac{\pi}{2}$. So, for this case equation (3.1) with $k = \pm\frac{\pi}{2}$ are the solitary wave-like solutions of equation (2.5). We further note that solitary waves have the maximum possible speed.
(2) l is odd and only odd values of j in the sum in the Hamiltonian, H, are permissible. Also, in this case, only $|k| = \frac{\pi}{2}$ is allowed. So, equation (3.1) with these particular values of k are the solitary wave-like solutions of equation (2.5).
(3) l is even and only even values of j in the sum in equation (3.5) are permissible. In this case, there is no permissible value of k. So, equation (2.5) will not have any solitary wave-like solution.
(4) l is arbitrary and j takes odd values with at least one even value. In this case, even if l is odd, there is no permissible value of k. So, equation (2.5) has no solitary wave-like solution.
(5) There is only one term, say the lth term, in the sum in equation (3.5). In this situation, equation (3.1) describes the solitary wave-like solution of equation (2.5) with $2l$ permissible values of k which are already given.

We also note that when $|g_j| \ll 1$ for $j = 1, 2, \ldots, l$, equation (2.5) then can be treated as a perturbed ALDNLSE. In this situation, we can use the standard perturbation theory to investigate the soliton dynamics from equation (2.5). This aspect is considered next.

4. The perturbative soliton dynamics of equation (2.5)

The method is amply discussed in the literature [16, 17, 56]. In this method, it is assumed that the zeroth-order solution is the standard one-soliton solution of the ALDNLSE. It is further assumed that the effect of perturbation on the soliton dynamics can be adequately taken into consideration by allowing four parameters, namely x, k, μ and α, to vary adiabatically in time, τ. Application of the method to the N-AL equation gives for μ, k and x

$$\begin{aligned} S(\mu, x) &= \sum_{s=1}^{\infty} \frac{\frac{\pi^2 s}{\mu}}{\sinh \frac{\pi^2 s}{\mu}} \cos 2\pi s x \\ G(k, l, \mu) &= \sum_{j=1}^{l} g_j \frac{\cos^2 kj}{\sinh^2 \mu j} \\ G_1(k, l, \mu) &= 4\frac{\sinh^4 \mu}{\mu^2}[\mu \coth \mu - 1 - 2S(\mu, x)] \\ G_2(k, l, \mu) &= G_1(k, l, \mu)\frac{\partial G(l, k, \mu)}{\partial k} \\ \dot{\mu} &= 0 \end{aligned} \tag{4.1}$$

$$\dot{k} = -8\frac{\sinh^4 \mu}{\mu^2} G(k, l, \mu)\frac{\partial S(\mu, x)}{\partial x} \tag{4.2}$$

$$\dot{x} = -2\frac{\sinh \mu}{\mu}\frac{\partial \cos k}{\partial k} - G_2(k, l, \mu). \tag{4.3}$$

We first note that the famous Poisson sum formula is used to obtain $S(\mu, x)$ and $G(k, l, \mu)$ [16]. In the situation where $\cos kj = 0$ for all j, both $G(k, l, \mu)$ and $\frac{\partial G(l,k,\mu)}{\partial k}$ are zero. In this case, it is easy to see that $\dot{\mu}, \dot{k}$ and $\dot{x}$ are given by equations (3.2) and (3.4), respectively. Of course, for $\dot{x}$ only certain values of k for $k \in [-\pi, \pi]$ are allowed. Notwithstanding this, this case is, as expected, similar to the one-soliton solution of the ALDNLSE. We consider next the problem of an effective Hamiltonian.

4.1. An effective Hamiltonian

In order to derive an effective Hamiltonian for the dynamical system described by equations (4.2) and (4.3), we multiply these two equations by $\dot{x}$ and $\dot{k}$, respectively. Now, subtracting the first one from the second, we get

$$-\left[2\frac{\sinh \mu}{\mu}\frac{\partial \cos k}{\partial k} + 4\frac{\sinh^4 \mu}{\mu^2}[\mu \coth \mu - 1 - 2S(\mu, x)]\frac{\partial G(l, k, \mu)}{\partial k}\right]\dot{k} + 8\frac{\sinh^4 \mu}{\mu^2} G(k, l, \mu)\frac{\partial S(\mu, x)}{\partial x}\dot{x} = 0. \tag{4.4}$$

It is easy to see that equation (4.4) defines a constant of motion of the dynamical system. This constant can be called the effective Hamiltonian, $H_{\text{eff}}(x, k, \mu, l)$, of the system and from equation (4.4) we get

$$H_{\text{eff}}(x, k, \mu, l) = -2\frac{\sinh \mu}{\mu}\cos k - 4\frac{\sinh^4 \mu}{\mu^2}[\mu \coth \mu - 1 - 2S(\mu, x)]G(l, k, \mu). \tag{4.5}$$

Again, it is easy to see from equation (4.4) that

$$\dot{x} = \frac{\partial H_{\text{eff}}}{\partial k} \qquad \text{and} \qquad \dot{k} = -\frac{\partial H_{\text{eff}}}{\partial x} \tag{4.6}$$

Table 1. Nature of fixed points from linearization analysis.

$x_s = \frac{p}{2}$	$k_s = n\pi$	Nature of fixed points		
p	n	Region I	Region II	Region III
Even	Even	Saddle	Saddle	Saddle
Odd	Even	Centre	Centre	Centre
Odd	Odd	Saddle	Centre	Centre
Even	Odd	Centre	Centre	Saddle

together yield the original equations of $\dot{x}$ and $\dot{k}$. In the subsequent analysis, the $l = 1$ case, being physically the most relevant, is analysed. In another simplification, $S(\mu, x)$ is approximated by its most dominant first term. This simplification will not make any qualitative change in the dynamics.

4.2. The analysis of fixed points

To obtain the fixed points of the set of equations, namely equations (4.2) and (4.3), we set $\dot{x}_s = 0 = \dot{k}_s$. This then gives $(x_s, k_s) = \left(\frac{p}{2}, n\pi\right)$ where p and $n = 0, \pm 1, \pm 2, \ldots$. To find the phase portraits around these fixed points, we define $z_1 = x - x_s$ and $z_2 = k - k_s$. We define for convenience and clarity

$$\begin{aligned} A_0(\mu) &= \frac{\sinh \mu}{\mu} \\ A_1(\mu) &= A_0^2(\mu)(\mu \coth \mu - 1) \\ A_2(\mu) &= A_0^2(\mu)\frac{\frac{\pi^2}{\mu}}{\sinh \frac{\pi^2}{\mu}}. \end{aligned} \tag{4.7}$$

We further define

$$\begin{aligned} B_0(\mu, p) &= A_1(\mu) - (-1)^p 2A_2(\mu) \\ B_1(\mu, g_1, p, n) &= (-1)^n A_0(\mu) + 4g_1 B_0(\mu, p) \\ B_2(\mu, g_1) &= 16\pi^2 g_1 A_2(\mu). \end{aligned} \tag{4.8}$$

Now, because of our stated assumptions, we get

$$\dot{z}_1 = 2B_1(\mu, g_1, p, n)z_2 \qquad \dot{z}_2 = (-1)^p 2B_2(\mu, g_1)z_1. \tag{4.9}$$

This set of equations, in turn, yields

$$\frac{z_1^2}{B_1(\mu, g_1, p, n)} - (-1)^p \frac{z_2^2}{B_2(\mu, g_1)} = \text{constant}. \tag{4.10}$$

From equation (4.10), it is transparent that the system has only two types of fixed points. These are centres and saddle hyperbolic fixed points. An in-depth analysis of fixed points is included in appendix B. The result of our analysis is tabulated in table 1. We note that there are two important values of μ, namely $\mu_r(g_1, \text{odd } p)$, and $\mu_r(g_1, \text{even } p)$, and these are roots of $B_1(\mu, g_1, p, n)$. Furthermore, for a given value of $g_1 > 0$, $\mu_r(g_1, \text{even } p) > \mu_r(g_1, \text{odd } p)$. It is shown in figure 1. By region I is meant that $\mu < \mu_r(g_1, \text{odd } p)$. Regions II and III are respectively characterized by $\mu_r(g_1, \text{odd } p) \leqslant \mu < \mu_r(g_1, \text{even } p)$ and $\mu \geqslant \mu_r(g_1, \text{even } p)$.

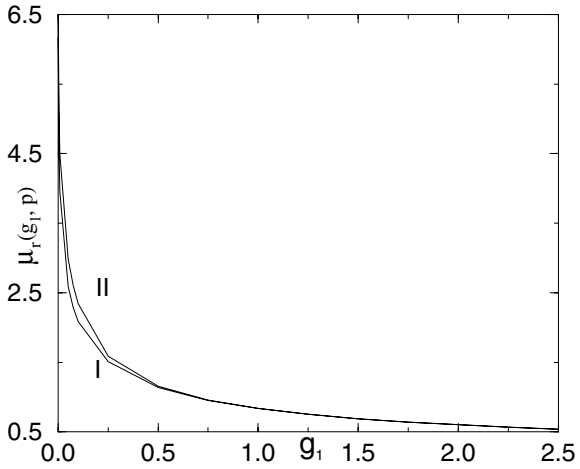

Figure 1. This shows the variation of $\mu_r(g_1, p)$ as a function of g_1 where μ_r is the root of $B_1(\mu, g_1, p, n)$ (equation (4.8) in the text). n is odd. I: p is odd and II: p is even.

4.3. A numerical analysis of phase portraits

Regarding the numerical investigation of phase diagrams around fixed points, we note that there are altogether 12 possibilities. Four possibilities arise from x_s and k_s being even or odd. Again, for each case, there are three possibilities, depending on the magnitude of μ. In this discussion, we consider $k_s = 0$ and π. Along the line $k_s = 0$ we have a set of fixed points at $x_s = 0, \pm\frac{1}{2}, \pm 1, \pm\frac{3}{2}, \pm 2, \ldots$. According to the analysis, based on linearization, $x_s = 0, \pm 1, \pm 2, \ldots$ should be saddle hyperbolic fixed points. Between every two consecutive saddle points, one should naturally expect centres. This is perfectly borne out in the numerical investigation (figure 2). It is also to be noted that figure 2 shows the phase diagram in the region I ($\mu < \mu_r(g_1, \text{odd } p)$). To understand the origin of a saddle fixed point between two consecutive centres, we note that two outermost ellipses encircling two centres will definitely touch at a point on the x-axis. Then, the flow of phase curves emanating from this point as well as in the vicinity of it will indicate a saddle hyperbolic fixed point. By a similar argument, the appearance of a centre between two consecutive saddle fixed points can be understood. It is also found that the absolute critical value of k, below which localization of a soliton occurs, increases monotonically with increasing μ. This behaviour is consistent with the physics of the problem.

We consider now the case of $k_s = \pi$. It has certain interesting twists, which is quite a common occurrence in the dynamics of nonlinear systems [58]. In region I, that is, $\mu < \mu_r(g_1, \text{odd } p)$, according to our standard linearization-based analysis, $x_s = 0, \pm 1, \pm 2, \ldots$ should be centres. On the other hand, $x_s = \pm\frac{1}{2}, \pm\frac{3}{2}, \ldots$ should be saddle hyperbolic fixed points. The reason to have a saddle hyperbolic fixed point between two consecutive centres has already been put forward in the previous paragraph. Our numerical investigation also confirms this result (figure 2). In region II ($\mu_r(g_1, \text{odd } p) \leqslant \mu < \mu_r(g_1, \text{even } p)$), the linearization analysis tells us that all fixed points along the line $k_s = \pi$ are centres. To understand this scenario, we note the following. Consider two centres, which are next but one to each other. Outermost ellipses encircling these fixed points can also intersect. We then have a convex lens-type region in the phase space (figure 3). Within this region of phase space, phase curves will have no other option but to close around a point on the x-axis.

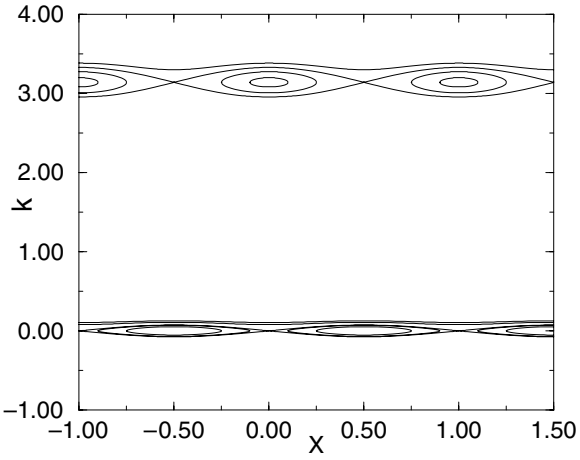

Figure 2. The bottom part of the figure is the phase portrait that shows the trapped and the moving solitons in region I for the fixed points having $k_s = 0.0$. For moving solitons, initial conditions are $\{x_s, k_{m0}\} = \{0.0, \frac{\pi}{40}\}$ and $\{0.0, \frac{\pi}{30}\}$, respectively. The upper part of the figure is the phase portrait that shows the trapped and the moving solitons in region I for the fixed points having $k_s = \pi$. For the moving soliton, $\{x_s, k_{m\pi}\} = \{0.5, \frac{21\pi}{20}\}$ is the initial choice. $\{x_s\}$ are shown in the figure. $l = 1$, $g_1 = 0.5$ and $\mu = 1.0$ for all curves in the figure. Equation (4.5) is used to obtain this phase portrait. (See also the text.)

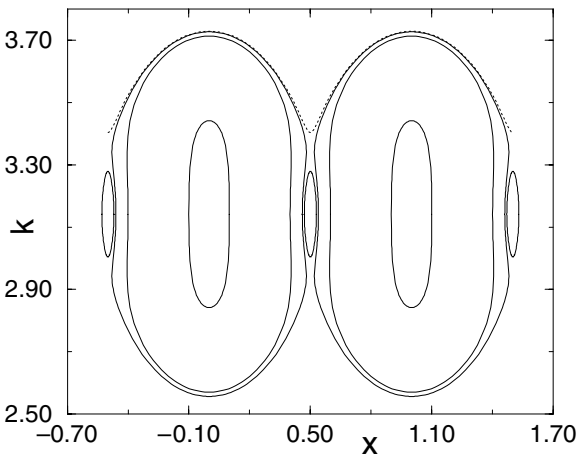

Figure 3. This phase portrait shows the trapped and the moving solitons in region II for fixed points having $k_s = \pi$. $\{x_s\}$ are, of course, shown in the figure. As per the text $l = 1$. Other parameters are $g_1 = 0.5$ and $\mu = 1.15$. For the moving soliton, the chosen initial point is $\{x_s, k_{m\pi}\} = \{0.5, \frac{13\pi}{12}\}$.

This fixed point will also then be another centre. This is clearly seen in figure 3, which describes the phase diagram of the soliton dynamics in the region II. It is needless to say that the phase diagram is very interesting and unique. To the best of my knowledge, this is the first case where a chain of centres with no hyperbolic fixed point is found along the line $k_s = \pi$, and more generally $k_s = (2l_2 + 1)$ where $l_2 = 0, \pm1, \pm2, \ldots$. We further note that the dotted curve in figure 3 has indeed the appearance of a heteroclinic orbit [57, 58], which in turn will also imply the existence of saddle points at $x_s = \frac{p}{2}$, where $p = \pm1, \pm2, \ldots$.

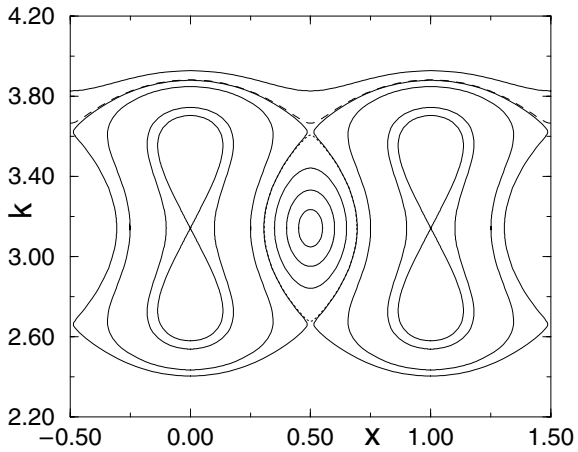

Figure 4. This phase portrait shows the trapped as well as the moving solitons in region III for fixed points having $k_s = \pi$. $\{x_s\}$ are, of course, shown in the figure. As per the text $l = 1$. Furthermore, $g_1 = 0.5$ and $\mu = 1.2$. For moving solitons, the chosen initial data are $\{x_s, k_{m\pi}\} = \{0.5, \frac{7\pi}{6}\}$ and $\{0.0, \frac{5\pi}{4}\}$, respectively.

So, it is to be noted that there are no saddle points in the region II, for $k_s = \pi$. The dotted curve in figure 3, albeit its appearance of a heteroclinic orbit, shows a marginally moving solitary wave, obtained by the perturbative method. This further implies that there will be moving solitary-wave solutions in this region too whenever k exceeds a critical value. This is discussed later in this section.

The phase diagram in region III is shown in figure 4. This region is defined by $\mu \geqslant \mu_r(g_1, \text{even } p)$. According to the linearization analysis, along the line $k_s = \pi$, $x_s = \pm\frac{1}{2}, \pm\frac{3}{2}, \ldots$ should be centres. This is indeed found in the numerical investigation. Again, the same linearization analysis tells that $x_s = 0, \pm 1, \pm 2, \ldots$ will be saddle hyperbolic fixed points. From the numerical study with $\mu = 1.2$ and $g_1 = 0.5$, we find that up to a certain distance from each of these fixed points, phase curves tend to diverge from the fixed points, indicating their hyperbolic structure. However, after a critical value of x, phase curves turn back to make closed curves. This happens up to a certain maximum value of x from the relevant fixed point on the line $k_s = \pi$. After that value of x, phase curves close around the nearest centre (figure 4). In case of $x_s = 0$, it is found that the phase curve with the initial value of x, $x_0 = 0.306$, closes around $x_s = 0$. But, for $x_0 = 0.307$, the phase curve encircles $x_s = 0.5$. So, for these two fixed points, the transition point is somewhere in between these two values.

It is important to realize that in this part of the problem, that is $\mu \geqslant \mu_r(g_1, \text{odd } p)$, we find four important phenomena that are encountered in nonlinear dynamics, namely (i) bifurcation, (ii) discrete breathers, (iii) inversion of stability and (iv) homoclinic connections [38, 57–60]. We note that for $\mu_r(g_1, \text{odd } p) \leqslant \mu < \mu_r(g_1, \text{even } p)$, that is, in region II, all saddle points are changed to centres (figure 3). So, we obtain a bifurcation in the phase portrait at $\mu = \mu_r(g_1, \text{odd } p)$. Furthermore it is a saddle-centre bifurcation. Again, at this bifurcation point, it is easy to show that we have spatially localized but time periodic solutions. These localized solutions can be pinned at one of the permissible values of x_s, namely at $x_s = \pm\frac{1}{2}, \pm\frac{3}{2}, \ldots$. These are, by definition, discrete breathers [38, 60]. To see it further, we examine equation (4.9). Since at $\mu = \mu(g_1, \text{odd } p)$, $B_1 = 0$, from the first equation of equation (4.9) we find that $\dot{z}_1 = 0$. The consistent solution is then $z_1 = 0$. This in

turn gives $x = x_s\ (\text{odd}\ p) = \left(l_1 + \frac{1}{2}\right)$ where $l_1 = 0, \pm 1, \pm 2, \ldots$. Then the second equation of equation (4.9) gives $\dot{z}_2 = 0$. This implies that $k = k_s = (2l_2 + 1)\pi$ where $l_2 = 0, \pm 1, \pm 2, \ldots$. For this particular case, $k_s = \pi$ or $l_2 = 0$. From the perturbative calculation of α appearing in equation (3.1) [17], it can be easily shown that α is proportional to $\tau = Jt$. The energy of the breather in terms of original variables [26] is

$$\tilde{E}[\mu_r(g_1, \text{odd}\ p)] = 1 + 2g_1 \frac{\sinh \mu_r(g_1, \text{odd}\ p)}{\mu_r(g_1, \text{odd}\ p)} \left[1 - \mu_r(g_1, \text{odd}\ p) \coth \mu_r(g_1, \text{odd}\ p) + \sum_{s=1}^{\infty} (-1)^s \frac{\frac{\pi^2 s}{\mu_r(g_1, \text{odd}\ p)}}{\sinh \frac{\pi^2 s}{\mu_r(g_1, \text{odd}\ p)}} \right] \tag{4.11}$$

$$E_{\text{breather}} = H[\mu_r(g_1, \text{odd}\ p)] = \frac{4J}{\lambda} \sinh \mu_r(g_1, \text{odd}\ p) \tilde{E}[\mu_r(g_1, \text{odd}\ p)].$$

We also note that for $\frac{J}{\lambda} > 0$, this is the minimum-energy spatially localized state. Inasmuch as equation (2.5) has a reflection symmetry, another discrete breather will be obtained by the transformation $g_1 \to -g_1$. This is discussed later.

We again note that our linearization analysis suggests that at $\mu = \mu(g_1, \text{even}\ p)$, we have another bifurcation. This time it is a centre-saddle bifurcation (figure 4). So, this model exhibits an important phenomenon of nonlinear dynamics, namely, 'inversion of stability'. It is also contextually important to note that in several other models the inversion of stability is observed by numerical simulations [39, 61]. On the other hand, our work provides a mathematically tractable model, which gives a deeper insight into the phenomenon.

We find that in region III the phase portraits around $x_s = 0, \pm 1, \pm 2, \ldots$ contain homoclinic connections or homoclinic orbits [57, 58]. Furthermore, in this region, for each saddle, there are two symmetrically placed homoclinic connections of saddle points connected to itself. Note that the orbits form a figure of eight around every saddle point (see figure 4) [57, 58]. We conclude this section by mentioning the following points. For $k_s = \pi$, in region I, saddles are connected by heteroclinic orbits (see the top of figure 2). On the other hand, in region III, every saddle point is connected to itself by homoclinic orbits (see figure 4). In other words, the dynamics of the system in the neighbourhood of saddle points is disconnected in region III. The other pertinent point to note from this perturbative analysis is that for all permissible values of μ and irrespective of the value of k_s, we get solitary wave-like solutions. This is quite different from what is found by the similar analysis in the DNLSE and the MSE [16, 17]. To understand the difference, we refer to figure 2. We note that both phase portraits in figure 2 arise due to chains of single minimum symmetric potential wells at $k_s = 0$, and π. This is actually true for all permissible values of k_s. However, minima of these potential wells at $k_s = 2l\pi$ align perfectly with maxima of potential wells at $k_s = 2(l + 1)\pi$, where $l = 0, \pm 1, \pm 2, \ldots$ and vice versa. In case of the DNLSE and the MSE, when $\mu = \mu_{\text{cr}}$, minima of these potential wells at $k_s = 2l\pi$ touch maxima of the potential wells at $k_s = (2l + 1)\pi$. So, when μ exceeds a critical value in these models, there is no region free of potential wells. Consequently, we cannot have any moving solitary wave-like solutions. When $\mu < \mu_{\text{cr}}$, we shall get both trapped and moving solitons in these models. On the other hand, in the present model, we must have a undistorted propagating solitary waves at $k = (2n + 1)\frac{\pi}{2}$, where $n = 0, \pm 1, \pm 2, \ldots$ for all values of μ (see equations (4.1)–(4.3)). This, in turn, prohibits the fusing of potential wells of the kind just mentioned. Hence, in this model there will be always a potential well-free region between two chains of potential wells. Consequently, in this model we shall always get propagating solitary wave-like solutions for all values of μ and k_s as seen in all phase portraits.

5. Stationary localized states

To study stationary localized states of equation (2.5), we seek an oscillatory solution of the form [26]

$$\Psi_m(\tau) = Q_m(\tau)\exp[\mathrm{i}(km - \omega\tau + \sigma_0)]\exp[-2\mathrm{i}\tau] \qquad m \in Z \tag{5.1}$$

where Q_m is real and σ_0 is a constant phase factor. From the real and imaginary parts of equation (2.5), we have

$$(\hat{\Omega}\hat{Q})_m = \omega Q_m + \cos k\big(1 + Q_m^2\big)(Q_{m+1} + Q_{m-1}) + 2\big(1 + Q_m^2\big)Q_m \sum_{j=1}^{l} g_j \cos^2 kj\big(Q_{m+j}^2 + Q_{m-j}^2\big) = 0 \tag{5.2}$$

$$\dot{Q}_m + \sin k\big(1 + Q_m^2\big)(Q_{m+1} - Q_{m-1}) = -2\big(1 + Q_m^2\big)Q_m \sum_{j=1}^{l} g_j \cos kj \sin kj\big(Q_{m+j}^2 - Q_{m-j}^2\big) \tag{5.3}$$

where $\hat{Q}$ is the column vector $(Q_1, Q_2, \ldots, Q_m, \ldots)$ and $\hat{\Omega}$ is the matrix defined by the left-hand side of equation (5.2). Equation (5.2) with vanishing boundary condition constitutes a nonlinear eigenvalue problem for localized states [10, 11, 26]. Equation (5.3) determines the time evolution of the localized states. It is a trite algebra to show that when $g_j = 0$ for all j, $Q_m(\tau)$ given by equation (3.1) is a solution of equations (5.2) and (5.3). When $k = 0$ or π, $Q_m, m \in Z$ is stationary. A localized state is called 'staggered' if $k = \pi$, and 'unstaggered' if $k = 0$. We further observe that under the transformation $Q_m \to (-1)^m Q_m$, equation (5.2) will remain invariant if $\omega \to -\omega$ and $g_j \to -g_j$ $j \in l$. This is indeed in accordance with the reflection symmetry of equation (2.5). This result in turn implies that if an unstaggered localized state, $Q_m \exp[-\mathrm{i}\omega\tau]$, is a solution of equation (5.2), the corresponding staggered localized state, $(-1)^m Q_m \exp[\mathrm{i}\omega\tau]$, is then a solution of the same, provided g_j, $j \in l$ changes sign for all j. To determine the locations of these localized states, we shall specialize on the $l = 1$ case. This simplification will not affect the merit of the discussion. From equation (5.2), we have

$$\omega = -2\cos k - (\cos k + 2g_1\cos^2 k)\frac{\sum_m Q_m^2(Q_{m+1} + Q_{m-1})}{\sum_m Q_m} - 2g_1\cos^2 k\frac{\sum_m Q_m^3\big(Q_{m+1}^2 + Q_{m-1}^2\big)}{\sum_m Q_m}. \tag{5.4}$$

We suppose that $Q_m > 0$, $m \in Z$ and $|g_1| \ll 1$. Then, the staggered state lies above the phonon band, while the unstaggered state lies below. We further note that when $\lambda \to 0$, $|g_1| \to \infty$. In this case, there is no localized state, staggered or unstaggered, below the phonon band if $g_1 < 0$, or above the phonon band for $g_1 > 0$.

The next important point is the effective mass of unstaggered and staggered localized states [16, 17, 26]. For this we consider the Hamiltonian, H_{eff}, given by equation (4.5). This consideration will allow us to obtain expressions for the effective mass for almost unstaggered and almost staggered states along with the fully unstaggered and fully staggered localized states [16, 17]. To calculate the effective mass of nearly unstaggered localized states, we let $k \to 0$ in equation (4.5). This in turn yields

$$\lim_{k\to 0} H_{\mathrm{eff}}(x, k, \mu) \sim \tfrac{1}{2}m_{\mathrm{eff}}^{-1}(x)k^2 - 2A_0(\mu) - 4g_1A_1(\mu) + 8g_1A_2(\mu)\cos 2\pi x + O(k^4) \tag{5.5}$$

where we define

$$m_{\rm eff}^{-1}(x) = 2A_0(\mu) + 8g_1A_1(\mu) - 16g_1A_2(\mu)\cos 2\pi x \tag{5.6}$$

and A_0, A_1 and A_2 are already defined in the text (see equation (4.7)). We note that $m_{\rm eff}(x)$ is an even function of both μ and x. It is to be noted that because of the proposed spatial dependence of $m_{\rm eff}$, this is a generalized definition of the quantity. Furthermore, by comparing equation (5.6) with equation (4.8), we find that $m_{\rm eff}^{-1}(0) = 2B_1(\mu, g_1, \text{even } p, 0)$ and $m_{\rm eff}^{-1}\left(\frac{1}{2}\right) = 2B_1(\mu, g_1, \text{odd } p, 0)$. As n is even in this case, we know from our analysis of $B_1(\mu, g_1, p, n)$ (appendix B) that for the coupling constant $g_1 > 0$, the effective mass of unstaggered and nearly unstaggered states is positive definite.

To obtain the effective mass of staggered localized states, we put $k = \pi - \theta$ and then let $\theta \to 0$. This procedure gives

$$-m_{\rm eff}^{-1}(x) = 2A_0(\mu) - 8g_1A_1(\mu) + 16g_1A_2(\mu)\cos 2\pi x. \tag{5.7}$$

Consequently, we get from equation (5.7) that when $\mu \to 0, m_{\rm eff}^{-1}(x) \to -2$. Furthermore, $m_{\rm eff}^{-1}(0) = 2B_1(\mu, g_1, \text{even } p, 1)$ and $m_{\rm eff}^{-1}\left(\frac{1}{2}\right) = 2B_1(\mu, g_1, \text{odd } p, 1)$. So, depending on the value of $g_1 > 0$, there will be a critical value of μ, $\mu_{\rm cr}(g_1)$, such that for $|\mu| > |\mu_{\rm cr}(g_1)|$, staggered as well as nearly staggered localized states will have positive effective mass. In fact, equation (5.7) has both lower and upper critical values of μ, namely $\mu_{\rm cr}^{\rm l} = \mu_{\rm r}(g_1, \text{odd } p)$ and $\mu_{\rm cr}^{\rm u} = \mu_{\rm r}(g_1, \text{even } p)$, depending on whether $\cos 2\pi x = -1$ or 1 (see appendix B). Figure 1 also records the dependence of these critical points on g_1. For $0 < |x| < \frac{1}{2}$, $\mu_{\rm cr}^{\rm l} < \mu_{\rm cr}(g_1) < \mu_{\rm cr}^{\rm u}$. We note that when $|\mu - \mu_{\rm cr}(g_1)| \to 0$, $\left|m_{\rm eff}^{-1}(x)\right| \to 0$. This in turn implies that for μ in the ϵ-neighbourhood of $\mu_{\rm cr}(g_1)$, the system will have strongly localized staggered states. We further note from equation (3.1) that μ^{-1} gives the measure of the localization length. So, states for which $\mu \to 0$ in equation (3.1) have long localization lengths. We conclude from this analysis then that stationary staggered localized states in the vicinity of the upper phonon band edge will have negative effective mass.

6. A numerical study of equation (2.5)

6.1. A study of solitary wave-like solutions

For the purpose of numerical integration, we first replace $\Psi_m, m = 1, 2, 3, \ldots$ by $\Psi_m \exp(-2i\tau)$ in equation (2.5). Next we write $\Psi_m = \Psi_{1m} + \text{Im}\,\Psi_{2m}$. From equation (2.5), we then get

$$-\dot{\Psi}_{1m} = \left(1 + \Psi_{1m}^2 + \Psi_{2m}^2\right)\Bigg[(\Psi_{2(m+1)} + \Psi_{2(m-1)}) + 2\sum_{j=1}^{l} g_j\{(\Psi_{1m}\Psi_{1(m+j)} + \Psi_{2m}\Psi_{2(m+j)})\Psi_{2(m+j)} + (\Psi_{1m}\Psi_{1(m-j)} + \Psi_{2m}\Psi_{2(m-j)})\Psi_{2(m-j)}\}\Bigg] \tag{6.1}$$

$$\dot{\Psi}_{2m} = \left(1 + \Psi_{1m}^2 + \Psi_{2m}^2\right)\Bigg[(\Psi_{1(m+1)} + \Psi_{1(m-1)}) + 2\sum_{j=1}^{l} g_j\{(\Psi_{1m}\Psi_{1(m+j)} + \Psi_{2m}\Psi_{2(m+j)})\Psi_{1(m+j)} + (\Psi_{1m}\Psi_{1(m-j)} + \Psi_{2m}\Psi_{2(m-j)})\Psi_{1(m-j)}\}\Bigg]. \tag{6.2}$$

For the initial condition, we use [8]

$$\Psi_{1m}(\tau = 0) = \frac{\sinh\mu}{\cosh m\mu}\cos km \tag{6.3}$$

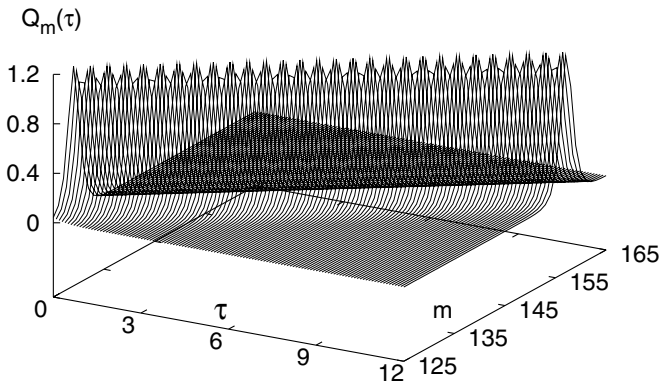

Figure 5. The N-AL dynamics of an initial Ablowitz–Ladik soliton with $k = \frac{\pi}{2}$ (equation (2.5)). Furthermore, $l = 1$, $g_1 = 0.5$ and $\mu = 1.0$. The number of sites in the chain is 257 and the origin is taken at the centre of the chain.

$$\Psi_{2m}(\tau = 0) = \frac{\sinh \mu}{\cosh m\mu} \sin km. \tag{6.4}$$

The fourth-order Runge–Kutta method is used to integrate these equations. The chosen time interval for all calculations is 10^{-4}. Furthermore, equation (2.4) with $\lambda = 1$ is used to check the accuracy of the integration. In this study, an one-dimensional lattice comprising 257 lattice points with unit lattice spacing is used. The initial condition is centred about the middle of the lattice, that is, about the 129th site. For the numerical analysis, we consider two cases, namely (i) $l = 1$ and (ii) $l = 2$ but $g_1 = 0$ in equation (2.5). For all cases that are presented in this section $\mu = 1$ and $g_j = 0.5$, $j = 1, 2$.

We note that in the first case the permissible values of k are $\pm\frac{\pi}{2}$ while for the second these values are $\pm\frac{\pi}{4}$ and $\pm\frac{3\pi}{4}$. For the first case, the absolute amplitude of the solitary wave-like solution (Q_m; see equation (3.1)) as a function of site and time (m, τ) is shown in figure 5 for $k = \frac{\pi}{2}$. Furthermore, for this case the time evolution of the absolute amplitude of the solitary wave ($Q_m(\tau)$) for some arbitrarily chosen sites, m, are shown in curves I, II and III in figure 6. For the second case $k = -\frac{3\pi}{4}$ is chosen and the spacetime evolution of $Q_m(\tau)$ is shown in figure 7. We note that in all cases the initial profile moves undistorted. These pictures are, as expected, identical to the spacetime evolution of the pure AL solitons. This is also verified by numerical integration.

6.2. A study of the PN pinning of solitary waves

Another important aspect that we study numerically here is the effect of the PN potential, which arises due to the nonintegrability term in equation (2.5) on the spacetime evolution of the initial profile given by equations (6.3) and (6.4) [26, 41, 42, 46]. We note that the nonintegrability effect is maximum when $k = 0$ in equation (3.1). On the other hand, it totally vanishes at $|k| = \frac{\pi}{2}$ for $l = 1$. We study again the propagation of an initial profile for $l = 1$, but with $\mu = 1.0$ and $g_1 = 0.5$. The accuracy of the integration is checked by the constancy of $\mathcal{N}$ (equation (2.4)). It is found that the loss of constancy becomes more and more discernible as $\left||k| - \frac{\pi}{2}\right| \to \frac{\pi}{2}$. This makes the simulation for small values of k less reliable. Figure 8 shows the spacetime evolution of $Q_m(\tau)$ (equation (3.1)) for $k = \frac{\pi}{3}$. We note that both the dispersion and the distortion of the initial profile are very transparent in figure 8. For better understanding, we also show through curves I(a)–III(a) in

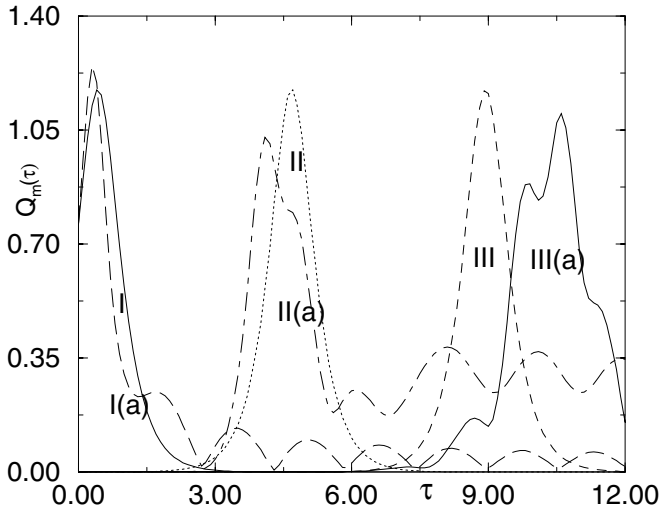

Figure 6. The N-AL equation (equation (2.5)) determined time evolution of $Q_m(\tau)$ (equation (3.1)) for some chosen values of sites m. $k = \frac{\pi}{2}$ and $\frac{\pi}{3}$, respectively. For both cases $l = 1$, $g_1 = 0.5$ and $\mu = 1.0$. The number of sites in the chain is 257 and the origin is taken at the centre of the chain. I, I(a): $m = 130$; II, II(a): $m = 140$; III, III(a): $m = 150$. The (a) series is for $k = \frac{\pi}{3}$ while the other one is for $k = \frac{\pi}{2}$.

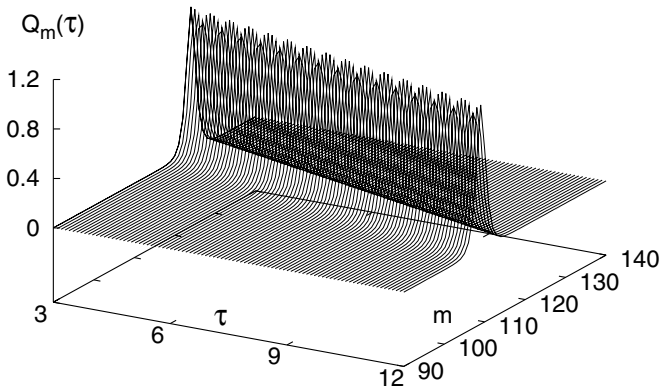

Figure 7. The N-AL dynamics of an initial Ablowitz–Ladik soliton with $k = -\frac{3\pi}{4}$ (equation (2.5)). Furthermore, $l = 2$, $g_1 = 0.0$, $g_2 = 0.5$ and $\mu = 1.0$. The number of sites in the chain is 257 and the origin is taken at the centre of the chain.

figure 6 and I(a)–IV(a) in figure 9 the time evolution of the $Q_m(\tau)$ for some arbitrarily chosen site or m values for $k = \frac{\pi}{3}$ and $\frac{\pi}{4}$, respectively. We note that the distortion of the initial profile and the intensity of the phonon tail increase as k decreases from $\frac{\pi}{3}$ to $\frac{\pi}{4}$. This is, of course, in the expected direction. Furthermore, in both cases the initial profile slows down by leaving the phonon behind in the propagation. Through curves I–IV in figure 9 the time evolution of $Q_m(\tau)$ for the same values of m from the Ablowitz–Ladik equation are included for comparison. This slowing down is very transparent in figure 9. So, it is reasonable to assume that these moving profiles will ultimately be trapped. However, we do not observe the total trapping in our simulations, as seen, for example in IN-DNLS [26]. We possibly

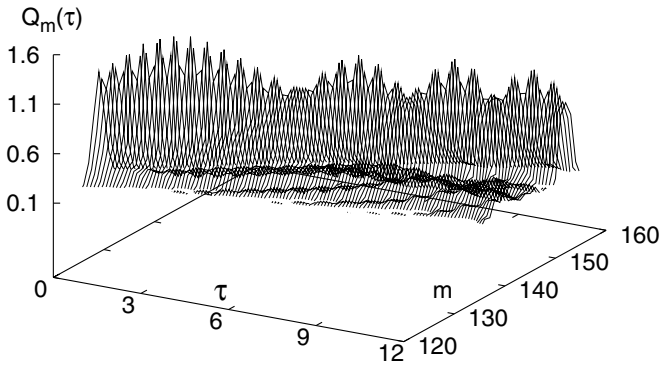

Figure 8. The N-AL dynamics of an initial Ablowitz–Ladik soliton with $k = \frac{\pi}{3}$ (equation (2.5)). Furthermore, $l = 1$, $g_1 = 0.5$ and $\mu = 1.0$. The number of sites in the chain is 257 and the origin is taken at the centre of the chain.

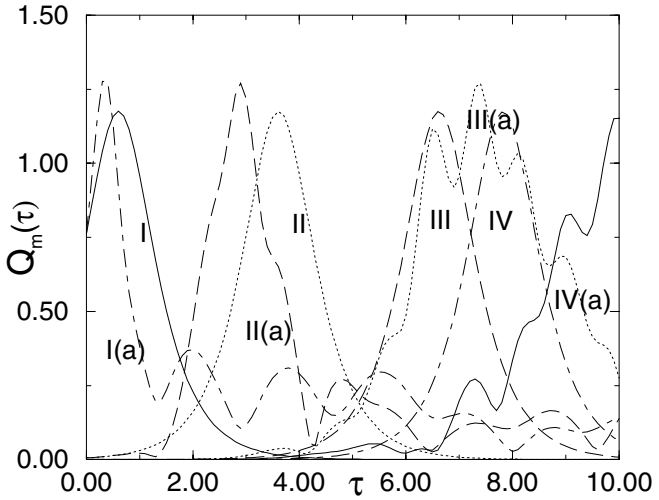

Figure 9. Same as figure 6, but with $k = \frac{\pi}{4}$ for both cases. I, I(a): $m = 130$; II, II(a): $m = 135$; III, III(a): $m = 140$; IV, IV(a): $m = 142$. While the (a) series is for the N-AL equation, the other one is for the Ablowitz–Ladik soliton.

need large integrability-breaking terms to see the total trapping in the time of the simulations. In the case of $k = \frac{\pi}{2}$, the nonintegrability term in equation (2.5) vanishes, and, as expected, the initial profile (equations (6.3) and (6.4)) propagates undistorted without any change in its speed and leaving no phonon tail behind as can be seen in figure 5 and curves I to III in figure 6.

6.3. A study of the interaction of two solitary waves

An important and also extensively studied field in nonlinear dynamics is the investigation and the understanding of the interaction of two or more solitary waves of nonintegrable nonlinear equations and the components of vector solitons in integrable nonlinear equations.

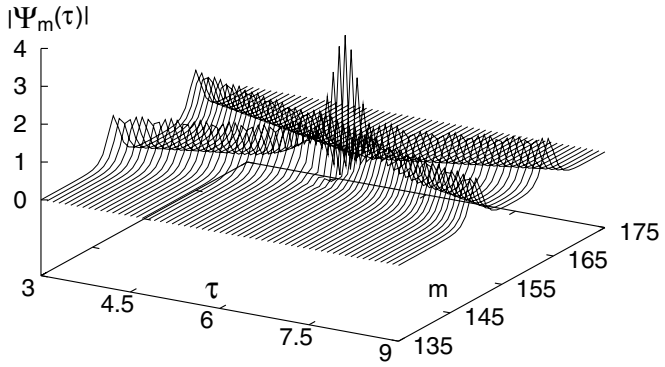

Figure 10. The N-AL collision dynamics of two initial AL pulses. $k_2 = -k_1 = \frac{\pi}{2}$. $l = 1$, $g_1 = 0.5$ and $\mu = 1.0$ as mentioned in the text. The number of sites in the chain is 313 and the origin is taken at the middle of the chain.

For this purpose, continuous nonlinear nonintegrable equations are studied extensively [25, 29–34, 40, 43, 48, 49]. In the case of discrete nonlinear nonintegrable equations, we note that the discrete nonlinear Klein–Gordon equation is used to study the collision of breathers and inelastic interaction of weak-amplitude phonons with breathers. Fission, fusion and spallation of breathers are found in these studies [40, 43, 62]. In this context, therefore, the N-AL equation (equation (2.5)) that is proposed here assumes a very great significance. This equation gives us further opportunity to study the interaction of solitary waves of a discrete nonlinear equation. To investigate this problem, as the initial condition we take the function [31, 32]

$$\Psi_m(0) = \frac{f_1 \sinh \mu}{\cosh[\mu(m - x_0)]} \exp[\mathrm{i}k_1(m - x_0] + \frac{f_2 \sinh \mu}{\cosh[\mu(m + x_0)]} \exp[\mathrm{i}k_2(m + x_0]. \tag{6.5}$$

We note that the function has two peaks at $x = x_0$ and $x = -x_0$, respectively. The velocity of the peak at x_0 is $\frac{\sinh \mu}{\mu} \sin k_1$ while the velocity of the other peak at $x = -x_0$ is $\frac{\sinh \mu}{\mu} \sin k_2$. We further note that when $|x_0| \to \infty$, equation (6.5) gives two AL-type solitons (equation (3.1)). This analysis is also done numerically using the fourth-order Runge–Kutta method, and the origin is placed at the centre of the one-dimensional chain. For all studies, we take $2|x_0| =$ 30 units, and $f_1 = f_2 = 1.0$.

The first one is as usual the $l = 1$ case. For this analysis we take for all cases $\mu = 1.0$ $g_1 = 0.5$. Inasmuch as $|k| = \frac{\pi}{2}$ in equation (3.1) is an exact one-soliton solution of equation (2.5), we consider first the case $k_2 = -k_1 = \frac{\pi}{2}$. In this case, we find that two peaks emerge after the collision without any change in shape and without any emission of a phonon (see also [30]). Of course, there can be phase shifts in these peaks after collision, but this is not investigated. This case of collision of solitons is shown in figure 10. We further note that the result is found to be independent of the value of g_1. But, we did not check the effect of changing μ on the collision. The other case that is considered is $k_1 = -\frac{\pi}{2.05}$ and $k_2 = \frac{\pi}{2}$. When $g_1 = 0$, we find that two solitons collide and after the collision again two peaks emerge without any change in shape and without any emission of a phonon. This is not shown here. On the other hand, when we give a nonzero value of g_1 (in our case 0.5), we find the fusion of two solitons on collision (see also [42]). Inasmuch as $k_2 = \frac{\pi}{2}$, the direction of the maximum velocity is in the direction of increasing lattice sites. The fused solution, as expected, moves in that direction. But, at the same time it emits phonons, as shown in figure11 [29].

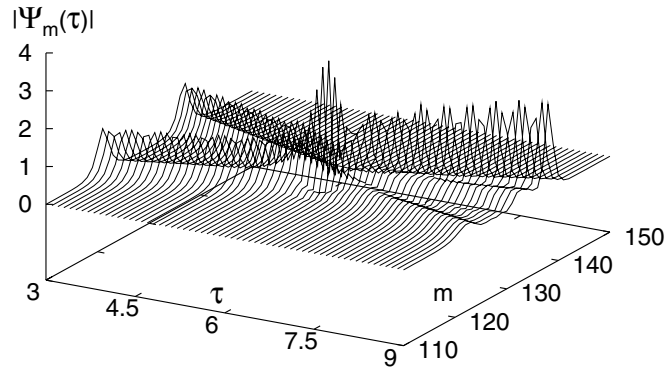

Figure 11. Same as in figure 10, but with $k_1 = \frac{\pi}{2.05}$ and $k_2 = -\frac{\pi}{2}$. $l = 1$, $g_1 = 0.5$ and $\mu = 1.0$. In this simulation, the number of sites is 257.

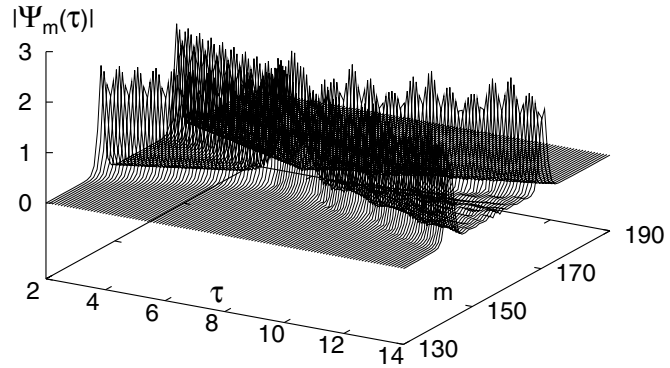

Figure 12. The N-AL collision dynamics of two initial AL pulses. $k_2 = -k_1 = \frac{3\pi}{4}$. $l = 2$, $g_1 = 0.0$, $g_2 = 0.5$ and $\mu = 1.5$ as mentioned in the text. The number of sites in the chain is 313 and the origin is taken at the middle of the chain.

The second case that we study is the case of $l = 2$, but $g_1 = 0.0$. In this case we have four permissible values of k, namely $k = \pm\frac{3\pi}{4}$ and $\pm\frac{\pi}{4}$. Of course, there are only two velocities, just as in the previous case. However, if we choose k_1 and k_2 from these allowed values of k, for $|x_0| \to \infty$, equation (6.5) will be the solution of equation (2.5). In this analysis, we choose $\mu = 1.5$, $g_2 = 0.5$ and $2|x_0| = 30$ units. For this case, the spacetime evolution of a solitary wave with $k = -\frac{3\pi}{4}$ is already shown in figure 7. In the first case we take $k_1 = -k_2 = -\frac{3\pi}{4}$ and the numerical simulation is shown in figure 12. In this case we see that two solitary waves do not pass each other. On the other hand, after coming close to each other, they are repelled. Other cases that are studied are $k_1 = -\frac{\pi}{4}$, but $k_2 = \frac{3\pi}{4}$, and $k_1 = -\frac{3\pi}{4}$, but $k_2 = \frac{\pi}{4}$, respectively. Our numerical simulations for these cases are shown in figures 13 and 14, respectively. In the first case, we see that two solitary waves fuse after collision and then move in the direction of positive velocity simultaneously emitting phonons. In the second case, however, we see the total destruction of the initial profile, equation (6.5), after the collision. This implies that there is no definite pattern in the collision process. Furthermore, the result of collision appears to be very sensitive to the phases of the colliding solitary waves. So, there should be attempts to understand this collision physics analytically, using the perturbative method and collective coordinate method [33].

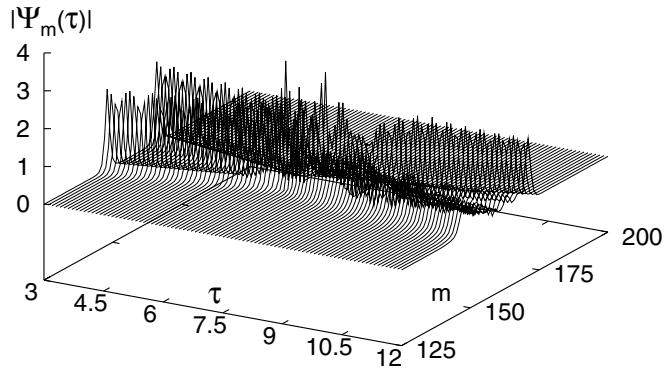

Figure 13. Same as in figure 12, but with $k_1 = -\frac{\pi}{4}$ and $k_2 = \frac{3\pi}{4}$. $l = 2$, $g_1 = 0.0$, $g_2 = 0.5$ and $\mu = 1.5$. In this simulation, the number of sites is 313.

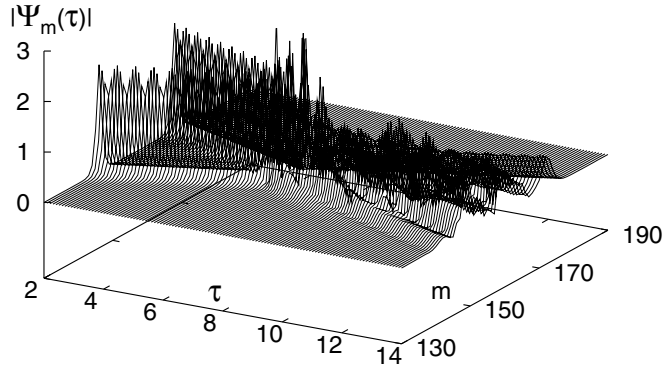

Figure 14. Same as in figure 13, but with $k_1 = -\frac{3\pi}{4}$ and $k_2 = \frac{\pi}{4}$. $l = 2$, $g_1 = 0.0$, $g_2 = 0.5$ and $\mu = 1.5$. In this simulation, the number of sites is 313.

7. Summary

A new class of nonintegrable Hamiltonians with tunable nonlinearities is proposed here to derive a class of (1 + 1)-dimensional nonintegrable discrete nonlinear Schrödinger equations, which include both some known nonlinear equations, such as the Ablowitz–Ladik nonlinear Schrödinger equation [6, 7], IN-DNLS [26, 50, 51] and a new subset, collectively christened as the N-AL equation (equation (2.5)). The relevant equations are obtained from the proposed Hamiltonian by the standard procedure of classical mechanics, but by employing a standard generalized definition of Poisson brackets, as shown in appendix A. In this paper, two cases of the N-AL equation are investigated analytically as well as numerically. These cases are (i) $l = 1$ and (ii) $l = 2$, but $g_1 = 0.0$ in equation (2.5).

An important characteristic of the N-AL equation is that it can allow spatially localized states of AL type (equation (3.1)) for certain permissible values of the parameter k to travel without distortion and without emitting phonons. This is found both analytically as well as numerically. So, these special solutions have in them the required balance of the nonlinearity and dispersion [5] and also are transparent to the PN potential arising from the lattice discreteness [26, 42, 46]. The transparency of these solutions to the PN potential

proves that these have the *continuous* translational symmetry of the one-soliton solution of the Ablowitz–Ladik equation (equation (3.1)) [26]. So, the N-AL equation provides another interesting example of nonintegrable discrete nonlinear equations which have solitary wave-like solutions [35].

Trapped and moving solitons are found from equation (2.5). This analysis is done using a standard perturbative procedure [16, 17]. The most interesting part of this analysis, however, is that it shows the existence of *saddle-centre bifurcations*. This in turn implies the presence of minimum-energy breathers in the system. Breathers are by definition time periodic, spatially localized solutions of equations of motion for classical degrees of freedom interacting on a lattice [38, 60]. We note that equations (4.1) satisfy these requirements. Since the saddle-centre bifurcation is seen in the perturbative method, it is, therefore, imperative to study the existence of breathers in the system numerically. We further note that in this system we also find a chain of centres. The origin of this situation is explained in the text. Along with the inversion of stability of fixed points [39, 61], we also observe the transformation of heteroclinic orbits to homoclinic orbits. Since phase portraits are very rich in characteristics, it is worthwhile to study them quite elaborately by extensively varying parameters such as μ and g_1 and also including more terms in $S(\mu, x)$ (equation (4.1)).

The presence of stable localized states in equation (2.5) is also investigated, albeit a more systematic analysis, presumably by the discrete variational method, is required. This work is indeed in progress. The effective masses of localized states are analysed here using the effective Hamiltonian given by equation (4.5) [16, 17]. It is found that nearly unstaggered as well as unstaggered localized states will always have positive effective mass. On the other hand, nearly-staggered and staggered localized states can have both negative and positive effective mass depending on the value of μ in equation (3.1). However, large-width but small-amplitude nearly staggered and staggered localized states do have the expected negative effective mass. Another important contribution in this section is to show the connection between the effective mass, m_{eff}, and the function, $B_1(\mu, g_1, p, n)$ (equation (4.8)), which determines the stability of fixed points.

It is further shown here numerically that all other solitary wave profiles (equations (6.3) and (6.4)) under the dynamics described by equation (2.5) and for which the nonintegrable term in equation (2.5) does not vanish, suffer distortion and emit phonons in the propagation. Further investigations along this line, by altering the strength of the nonintegrable term and the value of k, reveal that the extent of distortion and emission of phonons by the initial solitary wave profiles (equations (6.3) and (6.4)) depends on the magnitude of the nonintegrable term. We conclude from these two findings that any general solitary wave profile due to the presence of the nonintegrable term in equation (2.5) is subject to both the dynamical imbalance between the nonlinearity and the dispersion, and to the PN potential. This in turn implies that any such profile can either be trapped by emitting phonons or the localized structure will spread uniformly due to the effect of extra dispersion [5, 26, 42]. Notwithstanding the slowing down of initial profiles observed in our simulations, our numerical study in this matter, however, is not conclusive. So, a more elaborate study increasing the coupling constants in the nonintegrable term in equation (2.5) and also changing the parameter μ in equation (3.1) is needed. This will be done in future.

Finally, the N-AL equation (equation (2.5)), being a discrete nonintegrable nonlinear equation permitting solitary wave-like solutions, provides us with a golden opportunity to study an important phenomenon, namely the effect of both discreteness and nonintegrability on the collision dynamics of solitary wave profiles. Other contextually relevant studies are mentioned in the text [40, 43]. However, the noteworthy difference between our case and other cases lies in the use of initial conditions. Here only the collisions of two solitary wave

profiles are studied (equation (6.5)). In this study, we find that at least the interaction of two solitary wave profiles has some universal features, meaning that the outcome does not depend critically on the nature of the nonlinear equation. It is also equally true that we do not find so far any systematic pattern in the dynamics. It is, therefore, necessary to study this problem in detail both analytically and numerically to discern if there is any specific pattern in the dynamics. Another important aspect to study is the fractal structure of the emerging profile after the collision as a function of the initial velocity and the strength of the nonintegrable term [33, 34].

We conclude by noting that this study offers a very significant insight into the transport properties of the DHM. Furthermore, the N-AL equation can be used to study the transport properties of localized states in soft molecular chains, having the coexistence of nonlinearity and disorder, nonlinearity and quasiperiodicity or incommensurability in various parameters, such as the hopping integral, J, and the nonintegrable coupling constants, g_j, $j = 1, 2, \ldots$. Furthermore, the applicability of the N-AL equation in the study of exciton dynamics in photosynthesis and in molecular solids should be explored.

Appendix A. Generalized Poisson bracket

We consider a dynamical system having $2N$ generalized coordinates, $\{\phi_n, \phi_n^\star\}$, $n = 1, \ldots, N$. Let U and V be any two general dynamical variables of the system. We now define a nonstandard Poisson bracket [2]

$$\{U, V\}_{\{\phi,\phi^\star\}} = \sum_{n=1}^{N} \left(\frac{\partial U}{\partial \phi_n} \frac{\partial V}{\partial \phi_n^\star} - \frac{\partial V}{\partial \phi_n} \frac{\partial U}{\partial \phi_n^\star} \right) \left(1 + \lambda |\phi_n|^2\right). \tag{A1}$$

When $U = \phi_m$ and $V = \phi_l^\star$, we have [16, 26, 57]

$$\{\phi_m, \phi_l^\star\}_{\{\phi,\phi^\star\}} = \left(1 + \lambda |\phi_m|^2\right) \delta_{ml}. \tag{A2}$$

From equation (A1), we further have for $\{m, l\}$

$$\{\phi_m, \phi_l\}_{\{\phi,\phi^\star\}} = \{\phi_m^\star, \phi_l^\star\}_{\{\phi,\phi^\star\}} = 0. \tag{A3}$$

Then, when $U = \phi_m$ and $V = H$, we have from equation (A1)

$$\{\phi_m, H\}_{\{\phi,\phi^\star\}} = \left(1 + \lambda |\phi_m|^2\right) \frac{\partial H}{\partial \phi_m^\star}. \tag{A4}$$

We then write for the dynamical evolution of the mth generalized coordinate, ϕ_m[16, 26, 63]

$$\mathrm{i} \frac{\mathrm{d}\phi_m}{\mathrm{d}t} = \{\phi_m, H\}_{\{\phi,\phi^\star\}} = \left(1 + \lambda |\phi_m|^2\right) \frac{\partial H}{\partial \phi_m^\star}. \tag{A5}$$

This is consistent because

$$\begin{aligned} \mathrm{i} \frac{\mathrm{d}U}{\mathrm{d}t} &= \sum_{n=1}^{N} \left(\frac{\partial U}{\partial \phi_n} \mathrm{i}\dot{\phi}_n + \frac{\partial U}{\partial \phi_n^\star} \mathrm{i}\dot{\phi}_n^\star \right) = \sum_{n=1}^{N} \left(1 + \lambda |\phi_n|^2\right) \left(\frac{\partial U}{\partial \phi_n} \frac{\partial H}{\partial \phi_n^\star} - \frac{\partial U}{\partial \phi_n^\star} \frac{\partial H}{\partial \phi_n} \right) \\ &= \{U, H\}_{\{\phi,\phi^\star\}}. \end{aligned} \tag{A6}$$

We note now that when $U = H$, we have $\frac{\mathrm{d}H}{\mathrm{d}t} = 0$. In other words, H is a constant of motion. Consider $\mathcal{N}$ given by equation (2.4). To show that it is a constant of motion, we write $H = H_0 + H_1 - \frac{2}{\lambda}\left(\frac{\nu}{\lambda} - J\right)\mathcal{N}$, where we define

$$H_0 = J \sum_n \left(\phi_n^\star \phi_{n+1} + \phi_{n+1}^\star \phi_n\right) + \frac{2\nu}{\lambda} \sum_n |\phi_n|^2 \tag{A7}$$

$$H_1 = -\frac{1}{2}\sum_n \sum_{j=1}^{l} g_0^j \left(\phi_n^\star \phi_{n+j} + \phi_{n+j}^\star \phi_n\right)^2. \tag{A8}$$

We then find that

$$\mathrm{i}\frac{\mathrm{d}\mathcal{N}}{\mathrm{d}t} = \lambda \sum_n \left[\left(\phi_n^\star \frac{\partial H_0}{\partial \phi_n^\star} - \phi_n \frac{\partial H_0}{\partial \phi_n}\right) + \left(\phi_n^\star \frac{\partial H_1}{\partial \phi_n^\star} - \phi_n \frac{\partial H_1}{\partial \phi_n}\right)\right]. \tag{A9}$$

By using (A7) and (A8), it is very simple to show that the right-hand side of (A9) is zero. Hence, $\mathcal{N}$ is a constant of motion.

Appendix B. Analysis of fixed points

We note that $A_i(\mu), i = 0, 1, 2$ are even functions of μ; see equation (4.7). This, in turn implies that $B_i, i = 0, 1, 2$ are also even functions of μ; see equation (4.8). We take $g_1 > 0$ in this analysis. There will be no loss of generality by this assumption. We now note the following points.

(i) $B_0(\mu, p) \to 0$, as $\mu \to 0$. It can also be shown that $B_0(\mu, p)$ is a monotonically increasing function of μ. In other words, it is a monotonically increasing positive semidefinite function of μ. These properties are true, irrespective of p being even or odd.

(ii) $B_1(\mu, g_1, p, n) \to (-1)^n$, as $\mu \to 0$. Furthermore, it can be seen by plotting this function against μ that $B_1(\mu, g_1, p, n) > 0$, when $\mu \to \infty$. Both properties are true irrespective of the nature of p. Furthermore, when n is even, $B_1(\mu, g_1, p, n)$ is a monotonically increasing as well as a positive definite function of μ. On the other hand, when n is odd, there exists a value of μ, say $\mu_r(g_1, p)$ such that $B_1(\mu_r, g_1, p, n) = 0$. Again, $\mu_r(g_1, p)$ has the following properties: (a) for a given value of g_1, $\mu_r(g_1, \text{even } p) > \mu_r(g_1, \text{odd } p)$, (b) irrespective of the nature of p, the value of μ_r monotonically decreases with increasing g_1, and (c) $\mu_r(g_1, \text{even } p) \to \mu_r(g_1, \text{odd } p)$ as $g_1 \to \infty$; see also figure 1.

(iii) $B_2(\mu, g_1)$ is a monotonically increasing positive semidefinite function of μ.

We now consider each case to determine the nature of fixed points from the linearized analysis. We note that the classifications are done using standard analysis [51, 52].

Case I: n and p are both even. In this case, both $B_1(\mu, g_1, p, n)$ and $B_2(\mu, g_1)$ are positive. Equation (4.10) defines a hyperbola. So, the fixed point is a saddle point.
Case II: n is even, but p is odd. Since the nature of these two functions remains the same, equation (4.10) defines an ellipse. So, we have a centre.
Case III: Both n and p are odd. Again, $\mu > \mu_r(g_1, \text{even } p)$. In this case, both B_1 and B_2 are positive. So, equation (4.10) defines an ellipse and we have a centre.
Case IV: n is odd, but p is even. Furthermore, $\mu > \mu_r(g_1, \text{even } p)$. In this case also, both B_1 and B_2 are positive. But due to the evenness of p, equation (4.10) defines a hyperbola and we have a saddle point.
Case V: Both n and p are odd, but $\mu < \mu_r(g_1, \text{odd } p)$. In this case, while B_2 is positive, B_1 is negative. So, equation (4.10) defines a hyperbola and the fixed point is a saddle point.
Case VI: n is odd, but p is even. Again, $\mu < \mu_r(g_1, \text{odd } p)$. In this case, equation (4.10) defines an ellipse. So, we have a centre.
Case VII: Both n and p are odd. Again, $\mu_r(g_1, \text{odd } p) < \mu < \mu_r(g_1, \text{even } p)$. In this case, both B_1 and B_2 are positive. Since p is odd, equation (4.10) defines an ellipse. So, we have a centre.
Case VIII: n is odd, but p is even. Furthermore, $\mu_r(g_1, \text{odd } p) < \mu < \mu_r(g_1, \text{even } p)$. In this case, while B_1 is negative, B_2 is, however, positive. Since p is even, equation (4.10) defines

an ellipse. So, we have a centre. We also point out that same result will be obtained by examining two eigenvalues of the coefficient matrix.

References

[1] Drazin P G and Johnson R S 1989 *Solitons: An Introduction* (Cambridge: Cambridge University Press)
[2] Scott A 1999 *Nonlinear Science: Emergence and Dynamics of Coherent Structures* (Oxford: Oxford University Press)
[3] See e.g. Remoissenet M 1996 *Waves Called Solitons: Concepts and Experiments* (Berlin: Springer)
[4] Kivshar Yu S and Malomed B A 1989 *Rev. Mod. Phys.* **63** 761
[5] Sagdeev R Z, Meiseev S S, Tur A V and Yanevskii V V 1986 *Nonlinear Phenomena in Plasma Physics and Hydrodynamics* ed R Z Sagdeev (Moscow: Mir) p 137
[6] Ablowitz M J and Clarkson P A 1991 *Solitons, Nonlinear Evolution Equations and Inverse Scattering* (Cambridge: Cambridge University Press)
[7] Ablowitz M J and Ladik J L 1975 *J. Math. Phys.* **16** 598
Ablowitz M J and Ladik J L 1976 *J. Math. Phys.* **17** 1011
[8] Takeno S and Homma S 1991 *J. Phys. Soc. Japan* **60** 731
[9] Laedke E W, Spatschek K H and Turitsyn S K 1994 *Phys. Rev. Lett.* **73** 1055
[10] Ghosh A, Gupta B C and Kundu K 1998 *J. Phys.: Condens. Matter* **10** 2701
[11] Kundu K and Gupta B C 1998 *Eur. Phys. J.* B **3** 23
Gupta B C and Kundu K 2002 *Nonlinear Dynamics: Integrabilty and Chaos* ed M Daniel, K M Tamizhmani and R Sahadevan (New Delhi: Narosa) p 193
[12] Claude Ch, Kivshar Y S, Kluth O and Spatchek K H 1993 *Phys. Rev.* B **47** 14228
[13] Aceves A B, De Angelis C, Peschel T, Muschall R, Lederer F, Trillo S and Wabnitz S 1996 *Phys. Rev.* E **53** 1172
[14] Scott A C 1982 *Phys. Rev.* A **26** 578
[15] Yomosa S 1983 *J. Phys. Soc. Japan* **52** 1866
[16] Kundu K 2000 *Phys. Rev.* E **61** 5839
[17] Vakhnenko A A and Gaididei Yu B 1986 *Teor. Mat. Fiz.* **68** 350 (Engl. transl. 1987 *Theor. Math. Phys.* **68** 873)
[18] Takeno S 1992 *J. Phys. Soc. Japan* **61** 1433
[19] Hori K and Takeno S 1992 *J. Phys. Soc. Japan* **61** 4263
[20] Konotop V V and Takeno S 1997 *Phys. Rev.* B **55** 11342
Konotop V V and Takeno S 1998 *Physica* D **113** 261
[21] Kivshar Yu S, Pelinovsky D E, Cretegny T and Peyard M 1998 *Phys. Rev. Lett.* **80** 5032
[22] Davydov A S 1980 *Zh. Eksp. Teor. Fiz.* **78** 789 (Engl. transl. 1980 *Sov. Phys.–JETP* **51** 397)
[23] Bolterauer H 1990 *Davydov's Soliton Revisited, Self-Trapping of Vibrational Energy in Protein* ed P L Christiansen and A C Scott *(NATO ASI Series* vol 234) p 309
[24] Förner W and Ladik J 1990 *Davydov's Soliton Revisited, Self-Trapping of Vibrational Energy in Protein* ed P L Christiansen and A C Scott *(NATO ASI Series* vol 234) p 267
[25] Dmitriev S V, Kivshar Yu S and Shigenari T 2001 *Phys. Rev. Lett.* **64** 056613
[26] Cai D, Bishop A R and Grønbech-Jensen N 1994 *Phys. Rev. Lett.* **72** 591
[27] Johansson M and Kivshar Yu S 1999 *Phys. Rev. Lett.* **82** 85
[28] Zhou C, He X T and Chen S 1992 *Phys. Rev.* A **46** 2277
[29] Bullough R K and Caudrey P J 1980 *Topics in Current Physics: Solitons* ed R K Bullough and P J Caudrey (Berlin: Springer) p 6
[30] Aubry S 1976 *J. Chem. Phys.* **64** 3392
[31] Kudryavtsev A E 1975 *Pis. Zh. Eksp. Teor. Fiz.* **22** 178 (Engl. transl. 1975 *JETP Lett.* **22** 82)
[32] Getmanov B S 1976 *Pis. Zh. Eksp. Teor. Fiz.* **24** 323 (Engl. transl. 1976 *JETP Lett.* **24** 291)
[33] Anninos P, Oliveira S and Matzner R A 1991 *Phys. Rev.* D **44** 1147
[34] Yang J and Tan Yu 2000 *Phys. Rev. Lett.* **85** 3624
Yang J and Tan Yu 2001 *Phys. Lett.* A **280** 129
Tan Yu and Yang J 2001 *Phys. Rev.* E **64** 056616
[35] Friesecke G and Wattis J A D 1994 *Commun. Math. Phys.* **161** 391
[36] Toda M 1981 *Theory of Nonlinear Lattices Springer (Series in Solid-State Sciences vol 20)* (Berlin: Springer)
[37] Friesecke G and Pego R L 1999 *Nonlinearity* **12** 1601
Friesecke G and Pego R L 2002 *Nonlinearity* **15** 1343

[38] Marín J L and Aubry S 1996 *Nonlinearity* **9** 1501
[39] Marín J L, Aubry S and Floría L M 1998 *Physica* D **113** 283
[40] Cretegny T, Livi R and Spicci M 1998 *Physica* D **119** 88
[41] Cretegny T, Dauxois T, Ruffo S and Torcini A 1998 *Physica* D **121** 109
[42] Aubry S and Cretegny T 1998 *Physica* D **119** 34
[43] Bang O and Peyard M 1996 *Phys. Rev.* E **53** 4143
[44] Dunlap D H, Wu H-L and Phillips P 1990 *Phys. Rev. Lett.* **65** 88
[45] Kundu K, Giri D and Ray K 1996 *J. Phys. A: Math Gen.* **29** 5699
[46] Kivshar Y S and Campbell D K 1993 *Phys. Rev.* E **48** 3077
[47] Takeno S 1990 *Davydov's Soliton Revisited, Self-Trapping of Vibrational Energy in Protein* ed P L Christiansen and A C Scott *(NATO ASI Series* vol 234) p 31
[48] Stegeman G I and Segev M 1999 *Science* **286** 1518
Segev M and Stegeman G 1998 *Phys. Today* **51** 42
[49] Kanna T and Lakshmanan M 2001 *Phys. Rev. Lett.* **86** 5043
Anastassiou C, Segev M, Steiglitz K, Giordmaine J A and Mitchell M 1999 *Phys. Rev. Lett.* **83** 2332
[50] Salerno M 1992 *Phys. Rev.* A **46** 6856
[51] Konotop V V and Salerno M 1997 *Phys. Rev.* E **55** 4706
Konotop V V and Salerno M 1997 *Phys. Rev.* E **56** 3611
[52] Davydov A S and Kislukha N I 1976 *Zh. Eksp. Teor. Fiz.* **71** 1090 (Engl. transl. 1976 *Sov. Phys.–JETP* **44** 571)
[53] Rashba E I 1982 *Excitons* ed E I Rashba and M D Sturge (Amsterdam: North-Holland)
[54] Toyozawa Y 1983 *Molecular Aggregates (Springer Series in Solid-State Sciences* vol 49) ed P Reineker, H Haken and H C Wolf (Berlin: Springer)
[55] van Amerongen H, Valkunas L and van Grondelle R 2000 *Photosynthetic EXCITONS* (Singapore: World Scientific) chapter 6 pp 197–240
[56] Kaup D I 1976 *SIAM J. Appl. Math.* **31** 121
[57] Drazin P G 1992 *Nonlinear Systems* (Cambridge: Cambridge University Press)
[58] Alligood K T, Sauer T D and Yorke J A 1997 *Chaos: An Introduction to Dynamical Systems* (New York: Springer)
[59] Arrowsmith D K and Place C M 1982 *Ordinary Differential Equations* (London: Chapman and Hall)
[60] Flach S, Kladko K and MacKay R 1997 *Phys. Rev. Lett.* **78** 1207
[61] Campbell D K and Peyrard M 1990 *Chaos* ed D K Campbell (New York: AIP) p 305
[62] Cretegny T, Aubry S and Flach S 1998 *Physica* D **119** 73
[63] Das A 1989 *Integrable Models* (Singapore: World Scientific)